Bull. Mater. Sci., Vol. 37, No. 6, October 2014, pp. 1205–1214. © Indian Academy of Sciences.

Synthesis, characterization, photoluminescence and thermally stimulated luminescence investigations of orange red-emitting Sm^{3+}-doped $ZnAl_2O_4$ phosphor

MITHLESH KUMAR*, V NATARAJAN and S V GODBOLE

Radiochemistry Division, Bhabha Atomic Research Centre, Trombay, Mumbai 400 085, India

MS received 4 April 2013; revised 30 September 2013

Abstract. **Sm^{3+}-doped $ZnAl_2O_4$ phosphor was synthesized by citrate sol–gel method and characterized using X-ray diffraction and scanning electron microscopy to identify the crystalline phase and determine the particle size. Photoluminescence (PL) studies on the sample showed emission peaks at 563, 601, 646 and 707 nm with λ_{ex} = 230 nm corresponding to the $^4G_{5/2} \rightarrow {}^6H_{5/2}$, $^4G_{5/2} \rightarrow {}^6H_{7/2}$, $^4G_{5/2} \rightarrow {}^6H_{9/2}$ and $^4G_{5/2} \rightarrow {}^6H_{11/2}$ transitions, respectively, due to Sm^{3+} ions. PL lifetime decay studies confirmed that Sm^{3+} ions partly entered into the lattice by replacing Al^{3+} ions and remaining located at the surface of $ZnAl_2O_4$ host matrix. Thermally stimulated luminescence (TSL) studies of γ-irradiated Sm^{3+}-doped $ZnAl_2O_4$ sample showed two glow peaks at 440 and 495 K, the former being most intense than the latter. The trap parameters were determined using different heating rate methods. Spectral characteristics of the TSL glow showed emission around 565, 599 and 641 nm, indicating the role of Sm^{3+} ion as the luminescent centre. A probable mechanism for the prominent TSL glow peak, observed at 440 K, was proposed. CIE chromaticity coordinates for the system was evaluated, which suggested that Sm^{3+}-doped $ZnAl_2O_4$ could be employed as a potential orange red-emitting phosphor.**

Keywords. **$ZnAl_2O_4$; Sm^{3+} phosphor; photoluminescence; lifetime decay; thermally stimulated luminescence; colour coordinates.**

1. Introduction

Aluminum-based spinels are important oxide ceramic materials and have significant technological applications (Miron *et al* 2012). Among these compounds, $ZnAl_2O_4$ is employed in various catalytic reactions such as cracking, dehydration, hydrogenation and dehydrogenation in chemical and petrochemical industries (Shu Fen Wang *et al* 2005). The optical band gap of polycrystalline zinc aluminate is 3·8–3·9 eV. Due to its transparent and electroconductive properties, it can be used for ultraviolet (UV) photoelectronic devices. It is also used in optoelectronics, sensor technology and information display technology as efficient phosphor material for flat-panel displays because of its excellent optical, hydrophobic properties and high chemical, thermal stability (Xiang Ying Chen *et al* 2010). In the recent years, significant efforts have been devoted to study the luminescent properties of $ZnAl_2O_4$ doped with different impurity ions (Sanjay Mathur *et al* 2001; Sidorenko *et al* 2004; Olivera Milosevic *et al* 2005; Rusu *et al* 2009; Rafal *et al* 2012).

The rare earth ions consist of partially filled 4*f* shell that is well shielded by $5s^2$ and $5p^6$ orbitals and yield sharp lines in the optical spectra upon doping in inorganic materials (Feldmann *et al* 2003). Among the rare earth-doped hosts, samarium-doped compounds have a narrow line emission profile and a long lifetime similar to europium compounds (Valeria Moraes Longo *et al* 2010). Sm^{3+} ion has a $4f^5$ configuration and therefore is labelled as a Kramer ion due to its electronic states that are at least doubly degenerated level for any crystal field perturbation. Trivalent samarium has complicated energy levels and shows various possible transitions between *f*-energy levels. The transitions between these *f*-energy levels are highly selective and result in sharp line spectra. Sm^{3+} ions exhibit a strong orange-red fluorescence in the visible region. To gain information on possible stabilization of Sm^{2+} ions, the sample can be either γ-irradiated or calcined in reducing atmosphere for a few hours. The heat-treatment process in reducing atmosphere can be effective method for converting Sm from trivalent to divalent oxidation state (Zhiqiang Liu *et al* 2012). $ZnAl_2O_4$ can be used as a host matrix for trivalent rare-earth ions (e.g. Tb^{3+}, Eu^{3+} and Dy^{3+}) or transition metals (e.g. Mn^{2+} and Cr^{3+}) to prepare phosphors emitting mostly in the visible range of the electromagnetic spectrum (Tshabalala *et al* 2011). Sm^{3+}-doped $ZnAl_2O_4$ samples have been studied by earlier researchers for cathodoluminescence (CL) properties (Zhang *et al* 2002; Zhidong

*Author for correspondence (mithlesh010757@gmail.com)

Lou and Jianhua Hao 2004). Recently, the work on Eu^{3+}-doped $ZnAl_2O_4$ phosphor has been reported from our laboratory (Mithlesh Kumar *et al* 2012).

Significant efforts have been devoted towards the synthesis and characterization of rare-earth-doped $ZnAl_2O_4$ phosphors in the nano regime (< 100 nm). The luminescent properties are greatly dependent on the grain size, leading to attractive properties when the grain size decreases (Strek *et al* 2000). Therefore, sol–gel methods are efficient for the synthesis of nanophosphors, as they offer high purity, homogeneity, single phase and small and uniform particles size at relatively lower preparation temperature in comparison with other conventional methods (Zawadzki *et al* 2001). In this work, we have synthesized nano powders of Sm^{3+}-doped $ZnAl_2O_4$ by sol–gel method and characterized using X-ray diffraction (XRD) and scanning electron microscope (SEM) techniques. Subsequently, un-irradiated/γ-irradiated $ZnAl_2O_4 : Sm^{3+}$ and $ZnAl_2O_4$ phosphors were investigated using photoluminescence (PL), electron paramagnetic resonance (EPR) and thermally stimulated luminescence (TSL) techniques. These studies were done with a view to understand the local environment around Sm^{3+} ions by measuring intensity ratio of its electric dipole to magnetic dipole transitions and the substitution of Sm^{3+} ions in the $ZnAl_2O_4$ lattice. TSL and EPR results were combined to identify the trap/defect centres responsible for main glow peak observed in this system.

2. Experimental

2.1 *Sample synthesis*

Polycrystalline sample of Sm^{3+}-doped $ZnAl_2O_4$ was synthesized by the sol–gel method using citric acid as a chelating agent (Baochang Cheng *et al* 2006), starting with nitrates of the respective compounds. Stoichiometric quantities of zinc nitrate and aluminum nitrate were dissolved in quartz-distilled water and one mole percent of samarium nitrate was added to it. Stoichiometric amount of citric acid was added to it and then the mixed solution was heated at 353 K to form a highly viscous gel, which was calcined step-wise between 973 and 1173 K temperatures to get a fine powder. The process of grinding and then heating at 1173 K was repeated twice to obtain title compound. Undoped $ZnAl_2O_4$ phosphor was also prepared in a similar manner for comparison. The reaction of sample preparation can be described as follows

$$Zn(NO_3)_2 + 2Al(NO_3)_3 + C_6H_8O_7{\cdot}H_2O \rightarrow$$

$$ZnAl_2O_4 + 4N_2\uparrow + 6CO_2\uparrow + 1/2\ 11O_2\uparrow + 5H_2O.$$

A part of sample was further calcined at 1173 K in (Ar + 10% H_2) atmosphere for 5–6 h. The final product of $ZnAl_2O_4 : Sm^{2+}$ sample was obtained after second time grinding and heating in (Ar + 10% H_2) atmosphere.

2.2 *Sample characterization*

The as-synthesized products were characterized by XRD using CuKα-radiation with $\lambda = 1{\cdot}5418$ Å. The morphological investigations of the samples were carried out using SEM model AIS-2100: Merero Inc., South Korea. This was carried out on an instrument having both secondary electron detector and solid-state back-scattered electron detector. The micrographs were taken at 20 KeV acceleration voltages. PL excitation and emission spectra were recorded on an Edinburgh F-900 fluorescence spectrometer in the region 200–800 nm. The luminescence decay curve was recorded on a 20 ms scale with the pulse repetition rate at 10 Hz. The acquisition and analysis of the data were carried out by F-900 software supplied by Edinburgh Analytical Instruments, UK. All measurements were carried out at room temperature (Jain *et al* 2008). TSL investigations were carried out using home-built unit coupled to a personal computer in the range 300–600 K at different heating rates ($\beta = 1$, 2, 3 K/s) (Kadam *et al* 2008). TSL emission spectra were recorded using a Hitachi-2000 fluorescence spectrometer attached with heater assembly unit below the TSL glow temperature by 20 K. The details of instrument set-up for recording TSL emission spectra are described in the earlier paper (Mithlesh Kumar *et al* 2011). The samples of $ZnAl_2O_4 : Sm^{3+}$ and $ZnAl_2O_4$ were γ-irradiated using ^{60}Co source having a dose rate of 2 kGy/h.

3. Results and discussion

3.1 *Structural characterization*

The XRD pattern of Sm^{3+}-doped $ZnAl_2O_4$ phosphor is shown in figure 1. The crystallinity of the phosphors was

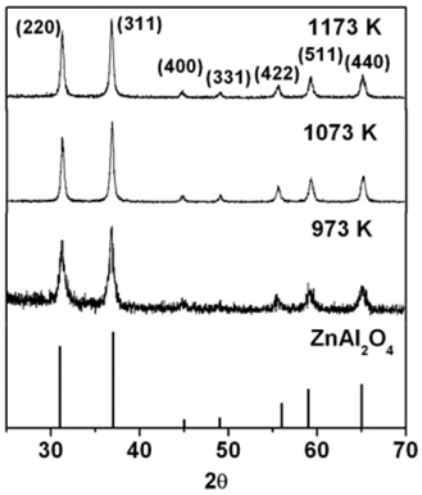

Figure 1. (**a**) XRD patterns of the $ZnAl_2O_4 : Sm^{3+}$ phosphor after 973, 1073 and 1173 K heat treatment. (**b**) ICDD stick pattern of $ZnAl_2O_4$ for card no. 05-0669.

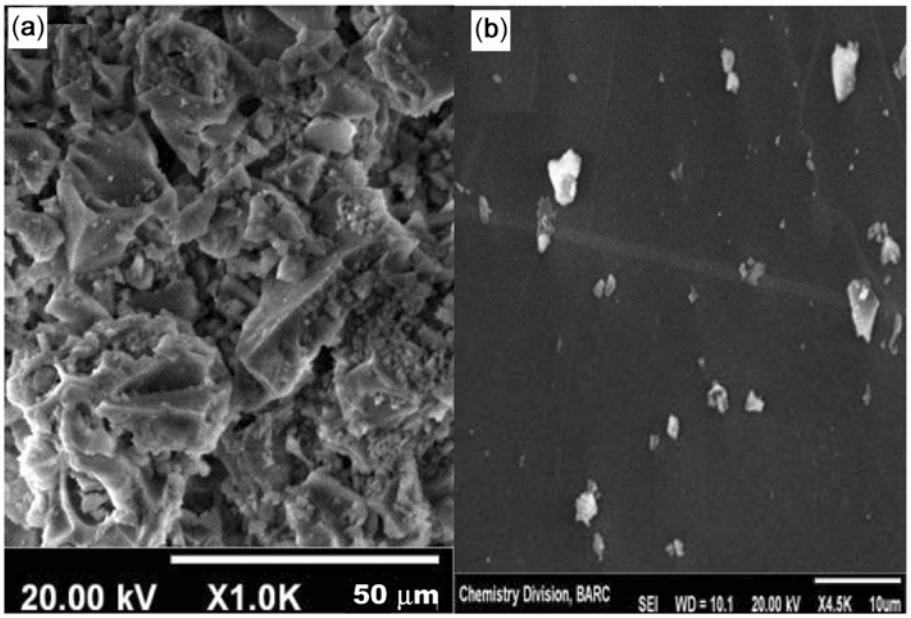

Figure 2. (**a**, **b**) SEM micrographs of $ZnAl_2O_4 : Sm^{3+}$.

checked by XRD technique as discussed earlier. All the peaks could be indexed well to the spinel $ZnAl_2O_4$ phase with literature value of cell parameter $a = 8{\cdot}059$ A. No impurity phase was observed. The XRD pattern was found to be in good agreement with that reported for the cubic $ZnAl_2O_4$ spinel (ICCD file no. 5-669). The observed diffraction peaks corresponded to the (2 2 0), (3 1 1), (4 0 0), (3 3 1), (4 2 2), (5 1 1) and (4 0 0) planes of cubic $ZnAl_2O_4$, respectively. Further, the refined lattice parameter of Sm^{3+}-doped $ZnAl_2O_4$ sample was calculated using least square computer program (Wadhavan 1972). The refined lattice parameter of $ZnAl_2O_4 : Sm^{3+}$ was found to be $a = 8{\cdot}0826(3)$ A. This suggested that the increase in lattice parameter is most likely due to the presence of Sm^{3+} in $ZnAl_2O_4$ system. Subsequently, Sm^{3+} ion (ionic size = 95·8 pm with 6-coordination number) has to replace either Al^{3+} ion (ionic size = 53·5 pm with 6-coordination number) at octahedral sites or Zn^{2+} ion (ionic size = 60 pm with 4-coordination number) at tetrahedral sites in the $ZnAl_2O_4$ host lattice (Shannon and Prewitt 1969; Shannon 1976). This is discussed in detail later. The peaks of XRD pattern become sharper on annealing due to the increase in crystallite size. X-ray line broadening takes place because of different reasons like instrumental artefacts (non-monochromaticity of the source, imperfect focusing) crystallite size, and residual strain arising from dislocations, coherent precipitates, etc. The particle size from X-ray line broadening is determined using Scherrer's formula

$$B(2\theta) = \frac{0{\cdot}94\lambda}{L\cos\theta},$$

where L is the crystallite size, λ the wavelength (for CuKα-radiation and $\lambda = 1{\cdot}5418$ Å) and $B = \sqrt{(B_M^2 - B_S^2)}$ (B_M is the full width at half maximum of the sample and B_S the standard grain size of around 2 μm). Scherrer's formula indicates that peak width (B) is inversely proportional to crystallite size (L). As the crystallite size gets smaller, the peak gets broader. With increase in temperature, the size of crystallite increases and so (B) decreases (Gupta *et al* 2012). In case of $ZnAl_2O_4 : Sm^{3+}$ sample, the average crystallite size was calculated from the most intense X-ray line ($2\theta = 36{\cdot}835$) broadening using Scherrer's formula (Klung and Alexander 1962). The average value of particle size was found to be around 36 nm. Further, SEM images of $ZnAl_2O_4 : Sm^{3+}$ were recorded. SEM images of $ZnAl_2O_4 : Sm^{3+}$ sample are shown in figure 2(a and b). SEM studies showed that the particles tend to agglomerate forming small clusters with irregular shapes as can be observed from micrograph. Furthermore, the particle size is in wide distribution, the average size being about 100–150 nm in diameter. SEM micrographs show irregular and compact particle size of phosphors. Since particles consist of a large number of crystallites, the size obtained using SEM is expected to be greater than that obtained using Scherrer's formula, which gives the size of the crystallite. $ZnAl_2O_4$ belongs to a class of mixed-metal oxides called the spinels, which are commonly represented by AB_2O_4, where A and B are divalent (2+) and trivalent (3+) cations, respectively. In the normal spinel structure, the 3+ ions of Al occupy the octahedral site, while the 2+ ions of Zn occupy the tetrahedral site. The spinel compound has a close packed face centered cubic structure with Fd_3m space group symmetry, where each unit cell contains 32 oxygen atoms (Hill *et al*

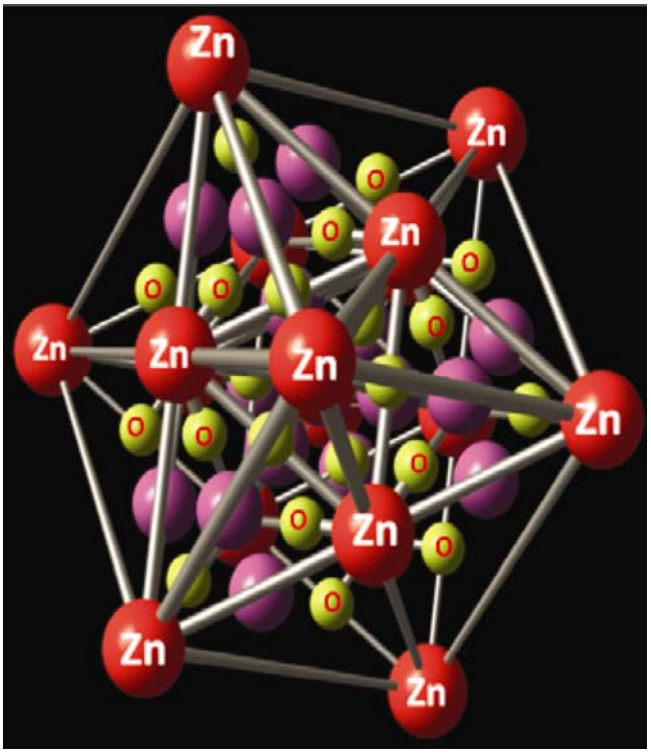

Figure 3. Schematic of the polyhedral crystal structure of $ZnAl_2O_4$.

1979; Levy *et al* 2001; Lopez-Moreno1 *et al* 2011). A schematic of the polyhedral network structure of the aluminate crystal is presented in figure 3. The polyhedral network structure was drawn using the Balls and Sticks visualization program (Ozawa and Sung J Kang 2004). With a view to confirm the incorporation of Sm in the host lattice, energy dispersive X-ray fluorescence (EDXRF) technique was used. The Sm content in the sample was found to be 0·80 mole%.

3.1a *PL investigations of $ZnAl_2O_4:Sm^{3+}$*: PL studies give information about the oxidation state of dopant ions and their lifetime parameters. In view of this, initially excitation and emission spectra were obtained on $ZnAl_2O_4:Sm^{3+}$ sample prepared between 973 and 1173 K. Figure 4(a) shows the excitation spectra of Sm^{3+}-doped $ZnAl_2O_4$ samples heated at 973, 1073 and 1173 K in the 200–400 nm range. As mentioned earlier, Sm^{3+} has complicated energy levels, which can lead to various possibilities of transitions among *f*-energy levels. The excitation spectra exhibited prominent peaks at 230, 247 and 260 nm with $\lambda_{em} = 601$ nm corresponding to the well-known excitation of Sm^{3+} ions (Chacon-Roa *et al* 2008; Xiaoming Liu and Jun Lin 2008). The positions of excitation peaks agree well with the reported values. All the peaks are due to the excitation from ground level $^6H_{5/2}$ to higher energy levels of Sm^{3+} ion. The most intense excitation peak was observed at 230 nm. Hence, for all further experimental purposes, 230 nm excitation wavelength was used. Figure 4(b) shows PL emission spectra of Sm^{3+}-doped $ZnAl_2O_4$ sample heated at 973, 1073 and 1173 K in 400–800 nm range. The emission spectra revealed fluorescence peaks at 563, 601, 646 and 707 nm with $\lambda_{ex} = 230$ nm. Blasse and Grabmaier (1994) have reported three dominant bands centered at 564, 602 and 644 nm and a weak emission in the region of 703 nm, which correspond to transitions from $^4G_{5/2}$ to $^6H_{5/2}$, $^6H_{7/2}$, $^6H_{9/2}$ and $^6H_{11/2}$ electronic energy levels, respectively, of Sm^{3+} ions. Yanlin Huang *et al* (2008a) have also reported stabilization of Sm^{3+} in $BaBPO_5$ in air-heated sample. This PL emission spectrum has exhibited fluorescence peaks at 563, 598, 644 and 703 nm, which are assigned to the $^4G_{5/2} \rightarrow {}^6H_{5/2}$, $^4G_{5/2} \rightarrow {}^6H_{7/2}$, $^4G_{5/2} \rightarrow {}^6H_{9/2}$ and $^4G_{5/2} \rightarrow {}^6H_{11/2}$ transitions, respectively, of Sm^{3+} ion. In the present case, PL emission peaks are very close to the reported peaks of Sm^{3+}-doped samples. Therefore, PL emission peaks at 563, 601, 646 and 707 nm of Sm^{3+}-doped $ZnAl_2O_4$ phosphor are assigned to the $^4G_{5/2} \rightarrow {}^6H_{5/2}$, $^4G_{5/2} \rightarrow {}^6H_{7/2}$, $^4G_{5/2} \rightarrow {}^6H_{9/2}$ and $^4G_{5/2} \rightarrow {}^6H_{11/2}$ transitions due to Sm^{3+} ions. The emission peak at 601 nm ($^4G_{5/2} \rightarrow {}^6H_{7/2}$) showed maximum intensity as compared to other emission peaks. Martinez-Sanchez *el al* (2005) have described that the magnetic dipole (md)-allowed transitions, which follows the selection rule $\Delta J = 0 \pm 1$. The transition $^4G_{5/2} \rightarrow {}^6H_{5/2}$, which is an (md) in nature and follows the first condition ($\Delta J = 0$) and whose intensity remains unchanged with the host matrix. The next transition $^4G_{5/2} \rightarrow {}^6H_{7/2}$ ($\Delta J = \pm 1$) is again an (md)-allowed one but is dominated by electric dipole (ed) transition. Therefore, it is partly an (md) and partly an (ed) natured one. The next transition $^4G_{5/2} \rightarrow {}^6H_{9/2}$ is purely an (ed) transition and is very sensitive to the crystal field (Annapurna *et al* 2003). Normally, the intensity ratio of (ed) to (md) transitions is used to measure the symmetry of the local environment of the trivalent 4*f* ions. The greater the intensity of (ed) transition, the more the asymmetric nature of the trivalent rare earth ions (May *et al* 1992). In $ZnAl_2O_4:Sm^{3+}$ system, the ratio of $^4G_{5/2} \rightarrow {}^6H_{9/2}$ (ed) and $^4G_{5/2} \rightarrow {}^6H_{5/2}$ (md) transitions is nearly 1·32, which gives a measure of the degree of distortion from the inversion symmetry of the local environment of the Sm^{3+} ion in the host. Therefore, the large asymmetry ratio value revealed strong electric fields of low symmetry at the Sm^{3+} ions. In addition, $^4G_{5/2} \rightarrow {}^6H_{9/2}$ (ed) transition in the electronic level of Sm^{3+} ions is more intense than $^4G_{5/2} \rightarrow {}^6H_{5/2}$ (md) transition and also indicated the asymmetric nature of Sm^{3+} ions. Therefore, it is suggested that Sm^{3+} is in a highly distorted environment. Moreover, a broad emission band peaking at 500 nm was observed. It is well known that Mn^{2+}-doped $ZnAl_2O_4$ phosphor exhibits broad PL emission in the visible region, peaking around 520 nm. Since a small amount of Mn^{2+} ions can be always present in the prepared $ZnAl_2O_4$ as an impurity, it is possible that the observed broad emission around 500 nm has some

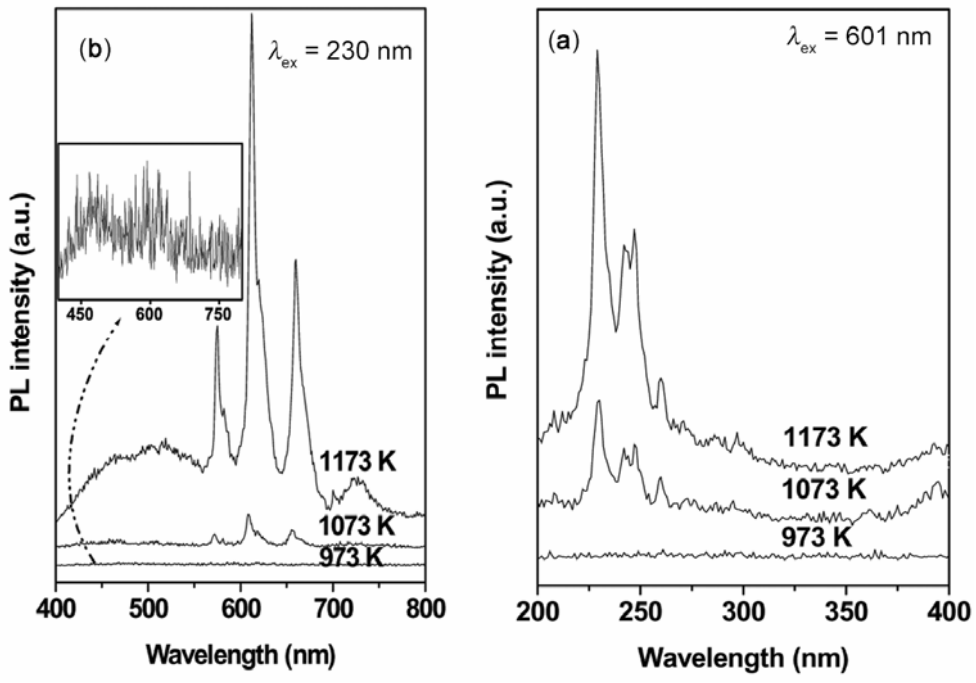

Figure 4. (**a**) PL excitation and (**b**) PL emission spectra of Sm^{3+}-doped $ZnAl_2O_4$ sample.

contribution from Mn^{2+} ions. A similar PL emission around 520 nm has been observed earlier in $ZnAl_2O_4$ nano-phosphors, wherein it was attributed to defect-mediated host lattice emission (Van Die *et al* 1987; Xiao-Jun Wang *et al* 2003). The PL emission at 500 nm has been also reported due to Mn^{2+} by Singh *et al* (2008), which corresponds to $^4T_1$–$^6A_1$ transition of Mn^{2+} ions. Therefore, we believe that the emission observed at 500 nm may be related to defect-mediated host lattice emission or due to Mn^{2+}. Further, EPR spectroscopy technique was used for the identification defect centres/ paramagnetic centres. The EPR results obtained on $ZnAl_2O_4 : Sm^{3+}$ sample are discussed later in §3.2e.

3.1b *Luminescence decay time studies*: Fluorescence decay time studies of Sm^{3+} ions in $ZnAl_2O_4$ were carried out to investigate the luminescence properties. Figure 5 shows the decay curve of Sm^{3+}-doped $ZnAl_2O_4$ phosphor for 601 nm ($^4G_{5/2} \rightarrow {}^6H_{7/2}$) emission peak with λ_{ex} = 230 nm. The luminescence decay curve was recorded on 20 ms scale between 10 and 3999 channel ranges. The exponential decay equation used for fitting is mathematically represented as

$$I(t) = A_1\exp(-t/\tau_1) + A_2\exp(-t/\tau_2) + A_0,$$

where I represents the fluorescent intensity; A_0, A_1, A_2 the scalar quantities; t the time of measurement and τ_1, τ_2 are the decay time values (i.e. the time taken for the excited state population to become 1/e of the original value). The decay curve could be well fitted into a bi-exponential decay, whose major component (80%) was τ_1 = 1·87 ms

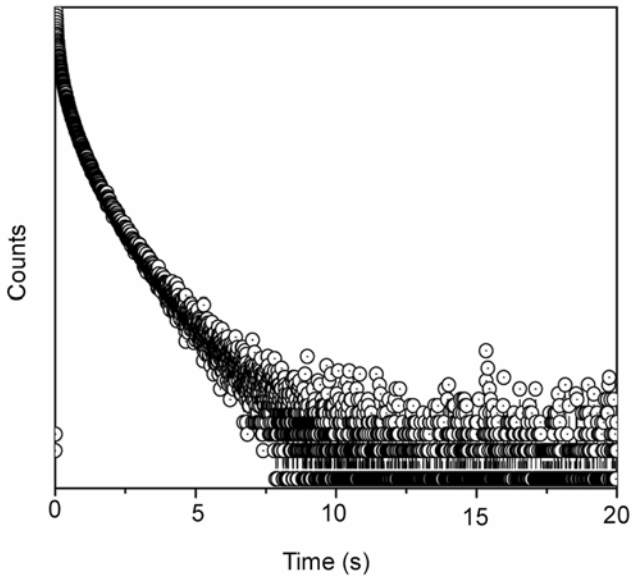

Figure 5. PL decay time profile of Sm^{3+}-doped $ZnAl_2O_4$ sample (heated at 1173 K) with λ_{ex} = 230 nm and λ_{em} = 601 nm.

and minor component (20%) was τ_2 = 0·48 ms. The PL decay rate is sum of the radiative and non-radiative decay rates as given below

$$\frac{1}{\tau_{PL}} = \frac{1}{\tau_R} + \frac{1}{\tau_{NR}},$$

where τ_{PL}, τ_R, τ_{NR} are the PL, radiative and non-radiative decay time constants, respectively. The surface defects in

nanostructure sample play an important role in influencing the luminescence properties (Zawadzki *et al* 2001; Xiang Ying Chen *et al* 2010). These findings suggested that Sm^{3+} ($4f^5$, $^6H_{5/2}$) ions are occupying two different sites in the $ZnAl_2O_4$ host lattice. Finally, Sm^{3+} ion has to enter into the host lattice by replacing Al^{3+}/Zn^{2+} sites or by locating on the surfaces of the crystallite of spinel structure system. However, Sm^{3+} having ionic size 95·5 pm is more likely to substitute at Zn^{2+} sites (ionic size = 60 pm) rather than at Al^{3+} sites (ionic size = 53·5 pm), if ionic size is the only criteria for substitution. But, it has been reported that the Sm^{3+} ions prefer sites with high coordination numbers, usually six or higher (Jain *et al* 1981). Since, in the present aluminate, the octahedral sites having the coordination number six are occupied by trivalent Al ions, in spite of the unusual size matching, these are the likely candidates for substitution by Sm^{3+} ions. However, due to large size mismatch, the resultant structure is not expected to be perfectly octahedral. Recently, another group of researchers has reported two sites of Sm^{3+} in BaFCl sample during annealing treatment. These authors have suggested that the first site is possibly located at or near the crystallite surface, whereas the second site is situated in a very ordered environment (Zhiqiang *et al* 2013). In the present work, it is believed that part of the Sm^{3+} ions might have entered into the lattice replacing Al^{3+} ions and the rest might be located at the surface of $ZnAl_2O_4$. Therefore, it can be pointed out that the asymmetric nature of the metal environment arises from the fact that Sm^{3+} ions, after replacing the Al^{3+} ion, will be in a much distorted geometry. Table 1 shows the lifetime values of different PL emission peaks of Sm^{3+}, which are very close to each other, suggesting that they belong to a single species. Further, time-resolved emission spectra (TRES) obtained to ascertain emission spectrum is due to Sm^{3+}. For this purpose, a set of emission scans was obtained by giving suitable delay times and choosing a proper time gate width with TRES data slicing range. The obtained spectra after a suitable time delay were found to be identical. These studies suggested that emission spectrum is due to Sm^{3+} alone. To evaluate the material performance on colour luminescent emission, CIE chromaticity coordinates were determined using standard procedures for $ZnAl_2O_4:Sm^{3+}$ sample (Publication CIE no. 17·4, publication CIE no 15·2). The values of x and y colour coordinates of the system were calculated to be 0·405 and 0·353, respectively. The CIE index for the $ZnAl_2O_4:Sm^{3+}$ phosphor is very close to the 'orange-red' line, which suggests that the present sample is a potential 'orange-red' emitting phosphor.

Table 1. Fluorescence decay time values for the $ZnAl_2O_4:Sm^{3+}$ sample with λ_{ex} = 230 nm.

λ_{em} (nm)	563	601	646
τ_1 (ms)	1·87	1·87	1·75
τ_2 (ms)	0·53	0·48	0·49

3.1c *PL investigations of γ-irradiated $ZnAl_2O_4:Sm^{3+}$:* Sm^{2+} ($4f^6$, $^7F_0$) ion-doped inorganic materials show relatively high thermal stability. As mentioned earlier, Sm^{3+} in $ZnAl_2O_4$ can be reduced to Sm^{2+} ions by heating in reducing atmosphere or by exposure to X-ray/γ-ray irradiation. No signal from Sm^{2+} ion was observed in freshly prepared phosphor. PL emission spectrum recorded on γ-irradiated Sm^{3+}-doped $ZnAl_2O_4$ phosphor (figure 6) showed bands at 563, 601, 646 and 707 nm and an additional group of bands at 676, 689, 698 and 709 nm with λ_{ex} = 230 nm. Normally, Sm^{3+} ions are stable in many host materials. It is also reported that several groups of narrow lines exist, whose lines are centred around 680, 689, 691 and 705 nm due to Sm^{2+} ions. The strongest fluorescent peak at 680 nm in these spectra is from the $^5D_0 \rightarrow {}^7F_0$ transition of Sm^{2+} and other bands were assigned to $^5D_0 \rightarrow {}^7F_1$ transitions of Sm^{2+} ions (Axe and Sorokin 1963). Other researchers have reported similar emission spectra of Sm^{2+} ions in different matrices, which were assigned the strongest fluorescent groups of $^5D_0 \rightarrow {}^7F_{0,1,2,3}$ transitions (f^6–f^6) of Sm^{2+} ions (George Belev *et al* 2011). In the present work, Sm^{3+}-doped $ZnAl_2O_4$, the emission spectrum recorded on γ-irradiated phosphor with dose = 2 KGy, has exhibited peaks due to Sm^{3+} (563, 601, 646 and 707 nm) and several additional weak lines centred around 676, 687, 698 and 709 nm. The strongest fluorescent peak (687 nm) in this spectrum is from the $^5D_0 \rightarrow {}^7F_0$ transition of Sm^{2+} and other bands

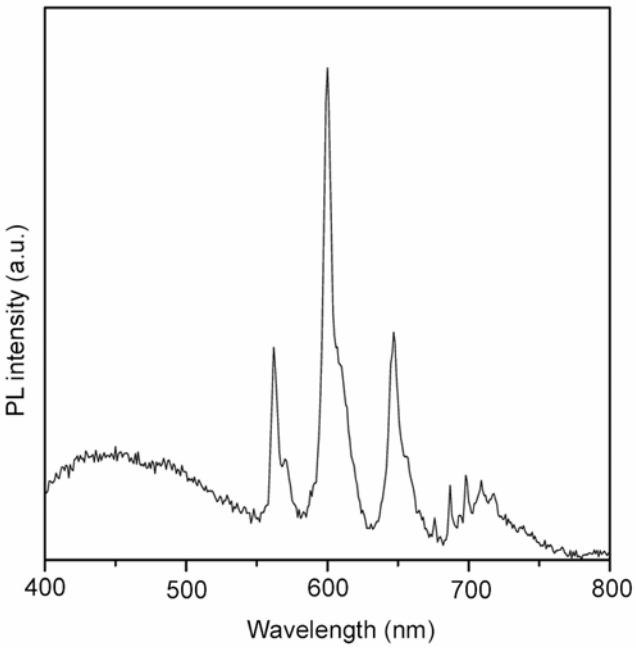

Figure 6. PL emission spectrum of γ-irradiated of Sm^{3+}-doped $ZnAl_2O_4$ sample with λ_{ex} = 230 nm.

698 and 709 nm, tentatively assigned to $^5D_0 \rightarrow {}^7F_1$ transitions of Sm^{2+} ions (Yanlin Huang *et al* 2008b). These experiments suggested that γ-irradiated phosphor exhibited the presence of Sm^{3+} as well as Sm^{2+} ions. However, the Sm^{2+} signal was very weak and marginally increased with higher doses. No significant reduction of Sm^{3+} signal in the form of PL intensity was noticed during build up of Sm^{2+} signal. The formation of Sm^{2+} ions was also observed in the samples prepared in (Ar + 10% H_2) atmosphere. Further, the lifetime observed for the latter group of emission was of the order of 15·90 ms and distinctly different from that of Sm^{3+} emissions, while no change in lifetime of Sm^{3+} emission (first group) was observed on γ-irradiation. These observations suggested that the additional emission bands observed on γ-irradiation are not due to Sm^{3+} ions. Hence, these emissions can be ascribed to the formation of Sm^{2+} ions by electron capture due to γ-irradiation.

3.1d *Annealing temperature dependence on the PL emission intensity*: PL investigations were carried out on Sm^{3+}-doped $ZnAl_2O_4$ phosphors calcined between 973 and 1173 K for several hours (figure 4(a and b)). The defects will be produced inevitably because of the partial/incomplete crystallization due to the rapid heat treatment process of the sample. Besides, the cation disorder in the spinel structure is considerable, so that there can be a great number of defects, which can serve as electron and/or hole trap sites. The defects are reduced drastically and the phosphor attains better crystallinity after the annealing treatment at higher temperature. It was seen that luminescence intensity increased significantly due to increasing temperature treatment at various stages and crystalline nature of the prepared phosphors was improved.

3.1e *EPR studies*: EPR experiments were conducted on Sm^{3+}-doped $ZnAl_2O_4$ phosphor at liquid nitrogen temperature (LNT). Figure 7 shows EPR spectrum of Sm^{3+}-doped $ZnAl_2O_4$ phosphor at LNT between 2 and 6 KG. There is a strong sextet signal with a hyperfine coupling constant of around 90 G at 3350 G ($g \cong 2$) corresponding to the free electron value. This is characteristic of Mn^{2+} ($^6S_{5/2}$ ground state) ions with d^5 configuration in an axially distorted state (Lou and Hao 2005; Vijay Singh *et al* 2008a, b). The EPR spectrum of Mn^{2+} ($I = 5/2$) ion is expected to exhibit five fine structure lines $-5/2 \leftrightarrow -3/2$, $-3/2 \leftrightarrow -1/2$, $-1/2 \leftrightarrow 1/2$, $1/2 \leftrightarrow 3/2$ and $3/2 \leftrightarrow 5/2$ for site symmetries other than cubic. However, in powder samples, due to large anisotropy, only the central line ($1/2 \leftrightarrow -1/2$) is usually observed along with its hyperfine splitting. Since a small amount of Mn^{2+} ions can be always present in the $ZnAl_2O_4$ as an impurity, these EPR signals might be associated with Mn^{2+} ions. The other intense EPR line centered around $g \approx 2$ between 3225 and 3375 G (150 G) was assigned due to a hole trapped at defect sites on basis of an earlier report (Singh *et al* 2012).

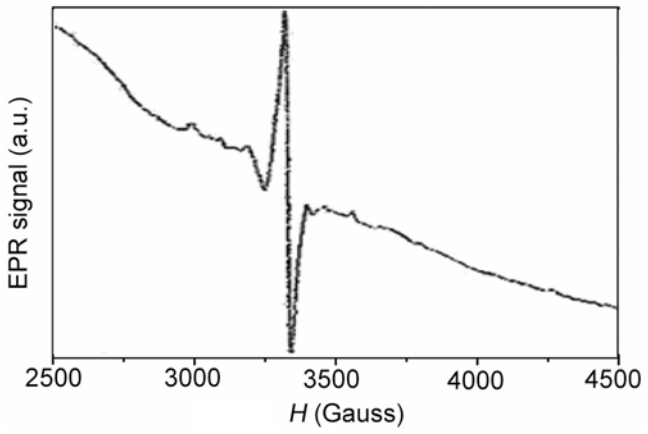

Figure 7. EPR spectrum of $ZnAl_2O_4 : Sm^{3+}$ sample at 77 K.

3.2 *Thermally stimulated luminescence studies*

Figure 8(a) shows the TSL glow curves of γ-irradiated Sm^{3+}-doped $ZnAl_2O_4$ and undoped-$ZnAl_2O_4$ samples at heating rate (β) = 3 K/s. The samples were γ-irradiated for the dose of 2 kGy. No glow curve was observed in undoped $ZnAl_2O_4$ and Sm^{3+}-doped $ZnAl_2O_4$ samples before γ-irradiation. The glow curve of γ-irradiated Sm^{3+}-doped $ZnAl_2O_4$ sample showed two peaks around 440 and 495 K. The peak at 440 K has higher intensity than the second peak at 495 K. The different heating rates method allows an estimate of trap parameter such as trap depth (E) and frequency factor (s). A change in the heating rate (β) produces a change in the maximum peak temperature (T_m). Plot of $\ln(T_m^2/\beta)$ vs $1/T_m$ yields a straight line, whose slope is found to be proportional to the trap depth and frequency factor. Experimentally, the glow curves were recorded at different heating rates (β) 1, 2 and 3 K/s and the plot of $\ln T_m^2/\beta$ against $1/T_m$ was obtained. A least-square-fit program was employed to obtain the best fit for E and s factors (Kiyak and Bulus 2001). Thermal bleaching of the lower temperature glow peak was done to get reliable trap depth value for higher-temperature TSL glow peak. The obtained plot is shown in the figure 8(b). The calculated trap parameters are listed in the table 2. TSL emission spectra were obtained on γ-irradiated $ZnAl_2O_4 : Sm^{3+}$ phosphor using a Hitachi-2000 fluorescence spectrometer at temperature 20 K below the TSL glow peak temperature 440 K (Kadam *et al* 2008). Figure 9 shows TSL emission spectrum recorded on γ-irradiated $ZnAl_2O_4 : Sm^{3+}$ sample in the 400–800 nm range. Spectral characteristics have shown emission around 565 ($^4G_{5/2} \rightarrow {}^6H_{5/2}$), 599 ($^4G_{5/2} \rightarrow {}^6H_{7/2}$) and 641 nm ($^4G_{5/2} \rightarrow {}^6H_{9/2}$) due to Sm^{3+} ions. TSL emission process depends not only on transition probabilities, but also on number of trapped

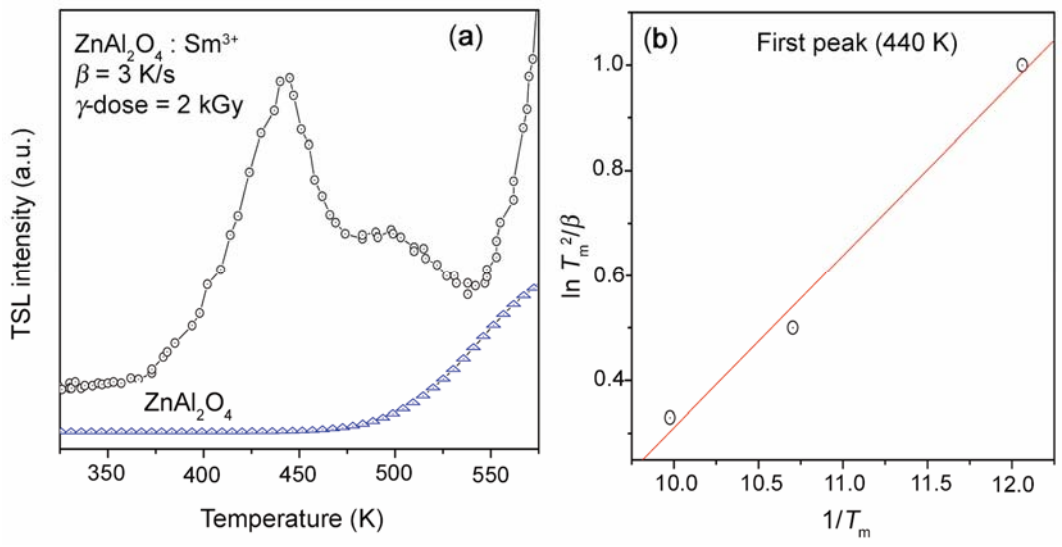

Figure 8. (**a**) TSL glow curves and (**b**) plot of $\ln T_m^2/\beta$ vs $1/T_m$ of the first peak (440 K) of $ZnAl_2O_4 : Sm^{3+}$ sample.

Table 2. Trap parameters.

Sl. no.	T_m (K)	E (eV)	S (s^{-1})
1	440	0·82	$4{\cdot}5 \times 10^{10}$
2	495	0·99	–

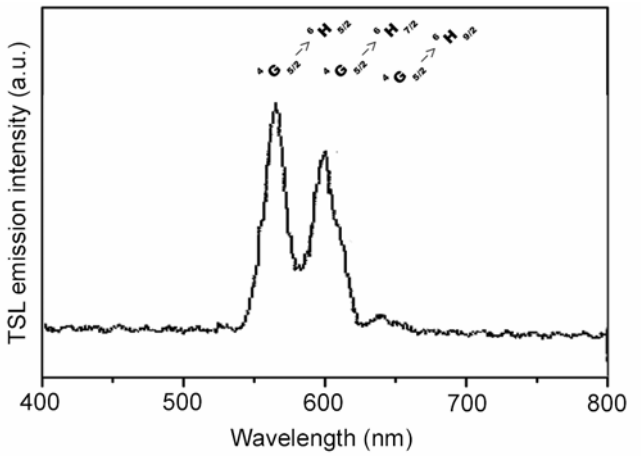

Figure 9. TSL emission spectrum obtained for $ZnAl_2O_4 : Sm^{3+}$ sample.

electrons/holes at various sites. These trapped electrons/holes decrease in number with time under isothermal heating conditions, due to continuous recombination and, thus, modify the spectral intensity at each wavelength position due to falling number density of recombination centres, which are responsible for the TSL excitation. Therefore, it is expected that TSL intensities of different emission peaks will decrease with increasing wavelengths. In the PL process, the luminescent ions are continuously excited under constant light flux, leading to intensity being recorded as a function of wavelength, which depends only upon the transition probability at each wavelength position. In addition, the changes in the relative intensities and width of the PL and TSL emission spectrum may be probably due to the difference in the relative sensitivities of the photomultiplier tube used in the PL and TSL experimental set-up. TSL and PL studies have confirmed that the Sm^{3+} ion acts as the luminescent centre in the TSL process.

The trapping centres or defect sites in a sample play a major role in the luminescence process. From the present experimental observations, the following probable mechanism for the glow peak at 440 K is proposed.

On γ irradiation

$ZnAl_2O_4 : Sm^{3+} \rightarrow$ electron, hole trapped centres, Sm^{2+}.

On heating at 440 K (TSL glow peak at 440 K)

Electron trapped centre + hole trapped centre $\rightarrow h\nu$,

Sm^{2+} + hole $\rightarrow Sm^{3+}$,

$Sm^{3+} + h\nu \rightarrow Sm^{3+}$* (excited state) $\rightarrow Sm^{3+}$ (TSL emission at 565, 599 and 641 nm).

The other TSL glow peak at 495 K could not be studied in detail due to its weak intensity.

4. Conclusions

$ZnAl_2O_4 : Sm^{3+}$ phosphor was prepared by a citrate sol–gel route. The particle size was determined to be around 36 nm. PL emission spectrum showed bands at 563, 601, 646 and 707 nm corresponding to the $^4G_{5/2} \rightarrow {}^6H_{5/2,7/2,9/2,11/2}$

transitions, respectively, due to Sm^{3+} ions. PL lifetime decay studies confirmed that Sm^{3+} ions partly entered into the lattice by replacing Al^{3+} ions and remaining located at the surface of $ZnAl_2O_4 : Sm^{3+}$. Sm^{2+} and electron/hole-trapped centres are identified in $ZnAl_2O_4 : Sm^{3+}$ phosphor. TSL and EPR studies have suggested that TSL glow peak observed at 440 K is associated with recombination of electron and hole centres through Sm^{3+} ions. The values of *x* and *y* colour coordinates of $ZnAl_2O : Sm^{3+}$ system are very close to the orange-red line.

Acknowledgements

The authors are grateful to Dr A Goswami, Head, Radiochemistry Division, BARC, for his keen interest and encouragement during the course of this work. The authors are thankful to Dr N D Dahale, Fuel Chemistry Division, BARC, Dr T K Seshagiri, former scientist, and Shri M Mohapatra, Radiochemistry Division, BARC, for their help during the course of this work.

References

Annapurna K, Dwivedi R N, Kundu P and Buddhudu S 2003 *Mater. Res. Bull.* **38** 429

Axe J D and Sorokin P P 1963 *Phys. Rev.* **130** 945

Baochang Cheng, Shengchun Qu, Huiying Zhou and Zhanguo Wang 2006 *Nanotechnology* **17** 2982

Blasse G and Grabmaier B C 1994 *Luminescence of materials* (Berlin: Springer)

Chacon-Roa C J, Guzman-Mendoza, Aguilar-Frutis M, Garcıa-Hipolito M, Alvarez-Fragoso O and Falcony C 2008 *J. Phys. D: Appl. Phys.* **41** 015104

Feldmann C, Justel T, Ronda C R and Schmidt P J 2003 *Adv. Funct. Matter* **13** 511

George Belev, Go Okada, Dancho Tonchev, Cyril Koughia, Chris Varoy, Andy Edgar, Tomasz Wysokinski, Dean Chapman and Safa Kasap 2011 *Phys. Status Solidi* **C8** 2822

Gupta S K, Mohapatra M, Kaity S, Natarajan V and Godbole S V 2012 *J. Lumin.* **132** 1329

Hill R J, Craig J R and Gibbs G V 1979 *Phys. Chem. Miner.* **4** 317

Jain A, Mohapatra M, Godbole S V and Tomar B S 2008 *Spectrochim. Acta. Part A* **71** 1007

Jain S R, Adiga K C and Vernek V P 1981 *Combust. Flame* **40** 71

Kadam R M, Seshagiri T K, Natarajan V and Godbole S V 2008 *Nucl. Instrum. Meth. Phys. Res.* **B266** 5137

Kiyak, N G and Bulus E 2001 *Radiat. Meas.* **33** 879

Klung H and Alexander L 1962 In *X-ray diffraction procedures* (New York, EUA: Wiley) p. 491

Levy D, Pavese A, Sani A and Pischedda V 2001 *Phys. Chem. Miner.* **28** 612

Lopez-Moreno S, Rodrıguez-Hernandez P, Munoz A, Romero A H, Manjon F J, Errandonea D, Rusu E and Ursaki V V 2011 *Ann. Phys.* (*Berlin*) **523** 157

Lou Z and Hao J 2005 *Appl. Phys.* **A80** 151

Martinez-Sanchez E, Garcia-Hipolito M, Guzman J, Ramos-Brito F, Santoyo-Salazar J, Martinez-Martinez R, Alvarez-Fregoso O, Ramos-Cortes M I, Mendez-Delgado J J and Falcony C 2005 *Phys. Status Solidi (a)* **202** 102

May P S, Matcalf D H, Richardson F S, Carter R C, Miller C E and Palmer R A 1992 *J. Lumin.* **51** 249

Miron I, Enache C, Vasile M and Grozescu I 2012 *Phys. Scr.* **T149** 014064

Mithlesh Kumar, Seshagiri T K, Mohapatra M, Natarajan V and Godbole S V 2012 *J. Lumin.* **132** 2521

Mithlesh Kumar, Seshagiri T K, Kadam R M and Godbole S V 2011 *Mater. Res. Bull.* **46** 1359

Olivera Milosevic, Lidija Mancic, Maria Eugenia Rabanal, Jose Manuel Torralba, Bairui Yang and Peter Townsend 2005 *J. Electrochem. Soc.* **152** G707

Ozawa T C and Sung J Kang 2004 *J. Appl. Cryst.* **37** 679

Publication CIE no. 17.4 1987 *International lighting vocabulary* (Vienna, Austria: Central Bureau of the Commission Internationale de L Eclairage)

Publication CIE no. 15.2 1986 Colorimetry (Vienna, Austria: Central Bureau of the Commission Internationale de L E clairage) 2nd edn

Rafal J Wiglusz, Tomasz Grzyb, Artur Bednarkiewicz, Stefan Lis and Wieslaw Strek 2012 *Eur. J. Inorg. Chem.* 3418

Rusu E, Ursaki V, Novitschi G, Vasile M, Petrenco P and Kulyuk L 2009 *Phys. Status Solidi.* **C6** 1199

Sanjay Mathur, Michael Veith, Michel Haas, Hao Shen, Nicolas Lecerf, Volker Huch, Stefan Hufner, Robert Haberkorn, Horst P Beck and Mohammad Jilavi 2001 *J. Am. Ceram. Soc.* **84** 1921

Shannon R D and Prewitt C T 1969 *Acta Crystallogr.* **B25** 925

Shannon R D 1976 *Acta Crystallogr.* **A32** 751

Shu Fen Wang, Feng Gu, Meng Kai Lu, Xiu Feng Cheng, Wen Guo Zou, Guang Jun Zhou, Shu Mei Wang and Yuan Yuan Zhou 2005 *J. Alloys Compd.* **394** 255

Sidorenko A V, Bos A J J, Dorenbos P, Evan Eijk C W, Rodnyi P A, Berezovskaya I V, Dotsenko V P, Guillot-Noel O and Gourier D 2004 *J. Phys.: Condens. Matter* **16** 4131

Singh V, Kumar Rai V, Watanabe S, Gundu Rao T K, Badie L, Ledoux-Rak I and Jho Y-D 2012 *Appl. Phys.* **B108** 437

Strek W, Deren P, Bednarkiewicz A, Zawadzki M and Wrzyszcz J 2000 *J. Alloys Compd.* **300–301** 456

Tshabalala K G, Cho S-H, Park J-K, Shreyas S Pitale, Nagpure I M, Kroon R E, Swart H C and Ntwaeaborwa O M 2011 *J. Alloys Compd.* **509** 10115

Valeria Moraes Longo, Maria das Grac, Sampaio Costa, Alexandre Zirpole Simoes, Ieda Lu cia Viana Rosa, Carlos Oliveira Paiva Santos, Juan Andres, Elson Longo and Jose Arana Varela 2010 *Phys. Chem. Chem. Phys.* **12** 7566

Vijay Singh, Natarajan V and Dong-Kuk Kima 2008a *Radiat. Effec. Defec. Solids* **163** 199

Vijay Singh, Chakradhar R P S, Rao J L and Dong-Kuk Kim 2008b *J. Lumin.* **128** 394

Van Die A, Chi Leenaers A, Vander Weg W F and Blasse G 1987 *Mater. Res. Bull.* **22** 781

Wadhavan V K 1972 *LATPAR, A least squares program* (Mumbai, India: Bhabha Atomic Research Center)

Xiang Ying Chen and Chao Ma 2010 *Opt. Mater.* **32** 415

Xiao-Jun Wang, Dongdong Jia and Yen W M 2003 *J. Lumin.* **102–103** 34

Xiaoming Liu and Jun Lin 2008 *J. Mater. Chem.* **18** 221

Yanlin Huang, Weifang Kai, Kiwan Jang, Ho Sueb Lee, Xigang Wang, Ying Zhang, Dake Qin and Chanfang Jiang 2008 *Mater. Lett.* **62** 1913

Yanlin Huang, Weifang Kai, Yonggang Cao, Kiwan Jang, Ho Sueb Lee, Ilgon Kim and Eunjin Cho 2008 *J. Appl. Phys.* **103** 053501

Zhang Q Y, Pita K, Ye W and Que W X 2002 *Chem. Phys. Lett.* **351** 163

Zhidong Lou and Jianhua Hao 2004 *Thin Solid Films* **450** 234

Zhiqiang Liu, Marion Stevens-Kalceff and Hans Riesen 2012 *J. Phys. Chem.* **C116** 8322

Zhiqiang Liu, Marion A, Stevens-Kalceff and Hans Riesen 2013 *J. Phys. Chem.* **A177** 1930

Zawadzki M, Wrzyszcz J, Strek W and Hreniak D 2001 *J. Alloys Compd.* **323–324** 279